

QUANTIFYING MACROPHAGE DEFECTS IN TYPE 1 DIABETES

Athanasius F. M. Marée^{1,3}, Mitsuhiro Komba², Cheryl Dyck², Marek Łabęcki¹
Diane T. Finegood² and Leah Edelstein-Keshet¹ *

¹ *Department of Mathematics and Institute of Applied Mathematics,
University of British Columbia, Vancouver, B.C., Canada*

² *Diabetes Research Laboratory, School of Kinesiology, Simon Fraser University, Burnaby, B.C., Canada*

³ *Current Address: Theoretical Biology/Bioinformatics, Utrecht University, Utrecht, the Netherlands*

17th October 2004

Keywords: macrophage phagocytosis, engulfment rate, digestion rate, activation rate, phagocytic index, percent phagocytosis, autoimmune diabetes, theoretical and experimental analysis.

Abstract

Macrophages from animals prone to autoimmune (type 1) diabetes differ from those of diabetes-resistant animals in processing and clearing apoptotic cells. Using *in vitro* time-course assays of the number of engulfed apoptotic cells observed within macrophages, we quantified these differences in non-obese diabetic (NOD) versus Balb/c mice. Simple models lead to several elementary parameter estimation techniques. We used these to compute approximate rates of macrophage engulfment and digestion of apoptotic cells from basic features of the data (such as initial rise-times, phagocytic index and percent phagocytosis). Combining these estimates with full fitting of a sequence of model variants to the data, we find that macrophages from normal (Balb/c) mice engulf apoptotic cells up to four times faster than macrophages from the diabetes-prone (NOD) mice. Further, Balb/c macrophages appear to undergo an activation step before achieving their high engulfment rate. In NOD macrophages, we did not see evidence for this activation step. Rates of digestion of engulfed apoptotic cells by macrophages are similar in both types. Since macrophage clearance is an important mechanism of disposal of self-antigen, these macrophage defects could potentially be a factor in predisposition to type 1 diabetes.

1 Introduction

Type 1 diabetes (T1D) is an autoimmune disease in which the insulin-producing β -cells in pancreatic islets are selectively destroyed. Numerous cells of the immune system, including CD8+ and CD4+ T cells, dendritic cells, and macrophages are known to play a part in the pathogenesis of T1D. Many chemical factors such as cytokines, are also implicated. This presents a complex system that is hard to untangle, where multiple effects are interrelated. In this paper, our goal is to learn more about one specific function of one class of cells, namely the phagocytosis of macrophages. Macrophages are the body's primary scavenger cells, and are responsible for clearing pathogens and apoptotic cells by phagocytosis. They also modulate the immune response by antigen presentation and activation of other immune cells (Gordon, 1998).

*Corresponding author: L. Keshet, Math Dept, UBC, Vancouver, BC V6T 1Z2, Canada; phone 604-822-5889; Fax 604-822-6074, email: keshet@math.ubc.ca

It has been shown that in young animals, the β -cell mass undergoes a stage of remodelling during which many cells enter programmed cell death (apoptosis). Defective clearance of these apoptotic β -cells by macrophages may lead to buildup of necrotic cells and debris which is collected and presented by dendritic cells to T cells in the pancreatic lymph nodes, initiating an autoimmune response. This idea is a current general hypothesis for the initiation of T1D from what would otherwise be normal cell turnover (Trudeau et al., 2000; Mathis et al., 2001).

It has indeed been shown that an aberrant response by macrophages is involved in the initiation of the disease (Georgiou et al., 1995; Shimada et al., 1994). Various defects have been observed in macrophages from non-obese diabetic (NOD) mice, including abnormal production of soluble mediators such as IL-12 (Alleva et al., 2000), less efficient activation of other immune cells (Jun et al., 1999), and reduced phagocytosis (O'Brien et al., 2002b).

Phagocytosis involves the engulfment and ensuing degradation of internalised material. After recognising and binding particles, macrophages are activated to release specific proteins, extend pseudopods and ingest the particles (Alleva et al., 2000). In previous *in vitro* assays we observed fewer apoptotic cells inside macrophages from diabetes-prone (NOD) compared with normal (Balb/c) mice (O'Brien et al., 2002b). This difference could be a consequence of upregulated degradation, of impaired engulfment, or of defective activation by NOD macrophages.

The approach is to do a comparative study *in vitro* of macrophages from animals that are prone to develop the disease versus those that are not. We combine an *in vitro* characterisation of the phagocytosis of apoptotic cells by macrophages with models that quantify the kinetics. The idea is that by learning about details of the function of these cells we could in future build up a more comprehensive understanding of the system as a whole. Modelling, experiments, and data analysis all play a fundamental role in this study.

We investigate which aspects of the macrophage phagocytosis (engulfment, degradation and/or activation) are altered in NOD mice, and quantify the level of impairment. To explore these differences quantitatively, we derive concise kinetic models for phagocytic uptake and digestion of apoptotic cells. We then use these models to compare macrophages isolated from NOD and Balb/c mice. In our models, we characterise macrophage classes according to the number of internalised apoptotic cells. This is similar to approaches in some previous papers, notably, Gammack et al. (2004) and Tran et al. (1995). Here, however, we also describe experiments in which each of these classes is measured, and we use the data to determine the best description of the process. Phagocytosis is assayed *in vitro* by feeding macrophages with apoptotic thymocytes, as described in Section 2.1, and (at fixed time points) counting the number of apoptotic cells visible within each of several hundred macrophages. The models described in this paper suggested experimental refinements that improved inferences about the underlying kinetic parameters. By fitting the kinetic models to the data, we estimate key parameters. We found differences in both activation and engulfment rates between the Balb/c and NOD macrophages, but not in digestion rates.

We use the models to mathematically derive shortcuts for calculating ball-park estimates of the kinetic parameters. Some of these are based on well-known and generally available indices such as *phagocytic index* and *percent phagocytosis*, commonly quantified in the literature (see definitions below). While full parameter fitting leads to greater accuracy, these basic methods can be helpful to biologists in interpreting data from other phagocytosis experiments. We also focus attention on detailed presentation of nonlinear parameter fitting techniques that allow us to compare between model variants, strains of mice, and distinct ways of grouping and analysing data points. We show that the Akaike Information Criterion can help to identify the models that are most parsimonious in terms of number of parameters while being optimal in terms of fit of the data.

2 Methods

2.1 Phagocytosis assay

5-week-old female Balb/c and NOD mice were purchased from Taconic (Germantown, NY). Animals were handled in accordance with the regulations of the Canadian Council on Animal Care and with approval by the Animal Care Committee at Simon Fraser University (Burnaby, BC). Macrophages were extracted from the mice by peritoneal lavage with cold complete medium (RPMI 1640, 100 U/ml penicillin/streptomycin, 10% v/v heat-inactivated fetal calf serum; Gibco Life Technologies, NY). Balb/c and NOD peritoneal macrophages were seeded into chamber slides (Nalge Nunc, IL) and incubated at 37°C / 5% CO₂ for 2 hours. To ensure that equal numbers of adherent macrophages among strains remained after washing, nonadherent cells from washes of single wells were regularly counted. The resulting initial number of adherent macrophages was approximately 10⁵ cells per well.

Suspensions of apoptotic cells were prepared by 20 min irradiation of mouse thymocytes using a short-wave (254 nm) ultraviolet C lamp (UVP, CA), followed by their incubation in serum-free complete medium at 37°C/5% CO₂ for 2 hours. Cell death was assessed using fluorescent microscopy and staining with fluorescein-isothiocyanate-labelled annexin V and with propidium iodide (PI) (Molecular Probes, OR). This yielded 44 ± 7% annexin V⁺/PI⁻ cells, which were classified as early apoptotic cells. Annexin V binds to phosphatidylserine molecules expressed on the surface of apoptotic cells, whereas PI serves as an indicator of membrane integrity, thus distinguishing apoptotic from necrotic cells.

Apoptotic cells were added to each well at the initial ratio of 5:1 apoptotic cells to adherent macrophages, and were cocultured with macrophages in 0.5 mL of a complete medium at 37°C/5% CO₂ for variable periods of time. Macrophages from multiple mice of a given strain (NOD or Balb/c) were mixed. Aliquots from this sample were seeded into 9 different wells. Each well was cultured for a distinct time period, e.g. 5, 10, 20, 30 min, and 1, 2, 4, 6, 8 hours, after which staining and counting took place. Figure 1 shows a typical image of macrophages with engulfed apoptotic cells. This set of nine measurements is referred to as “a single 8-hour time series”. (Note that we could not observe a true time series because staining kills macrophages.) The procedure was repeated 5 times, leading to 5 independent time series for each strain (using different aliquots), hereafter denoted 5 “replicates”. (In one time series, one mixture was cultured for 90 min instead of 5 min.) Before staining, a given well was washed three times with cold phosphate-buffered saline (PBS) to remove apoptotic thymocytes that had not been phagocytosed, and then macrophages were fixed in neutral buffered formalin (Sigma, MO). Cells were stained with hematoxylin and eosin (Sigma, MO), and observed using light microscopy at 1000-fold magnification under oil immersion.

Phagocytosis was evaluated by counting 150-1340 macrophages per well at the end of each culture period. (Altogether, 90 wells (45 per strain) were analysed, with a total of 86676 macrophages.) Each macrophage was assigned to a class ($i = 1, 2, \dots, N$) according to the number of internalised apoptotic cells it contained. Only apoptotic cells clearly visible within the perimeter of the macrophage were counted. The maximum number of apoptotic cells observed inside any given macrophage was 7. We used these observations to calculate the densities of macrophages in each of the classes, the percent phagocytosis, Φ (the number of macrophages containing at least one apoptotic cell per 100 macrophages), and the phagocytosis index, I_Φ (the number of ingested apoptotic cells per 100 macrophages). The remaining density of apoptotic cells, A , could not be measured. Because the number of cells observed per well varied greatly, we used densities, rather than absolute numbers of observed macrophages in a given class for all data analysis.

2.2 Model assumptions

We here model the process of macrophage encounter and engulfment of apoptotic cells. In the experiments, macrophages and apoptotic cells are randomly distributed, and macrophages can be assumed to move randomly. Furthermore, it is evident that “handling times” of apoptotic cells by macrophages during engulfment are very short (see Assumption 2), so it is reasonable to use mass-action kinetics to represent rates of encounter. We subdivide macrophages into classes according to their number of (visible) engulfed apoptotic cells. Let M_i be the density of macrophages that contain i visible engulfed apoptotic cells. The integer i ranges from 0 (none ingested) to some maximal observed value (i.e. 7 in our experimental data). Later, we will show that it is not essential to incorporate a maximal macrophage capacity, N , in the model analysis, because the probability of observing a macrophage with i internalised apoptotic cells decreases sharply with increasing values of i . However, for simulation-based full parameter fits to the models, we took $N = 7$, unless indicated otherwise. The kinetic model for the process of phagocytosis is based on the following assumptions:

1. Engulfment of apoptotic cells by macrophages takes place with mass-action kinetics, sequentially with a constant rate, described by a parameter k_e . (This is an approximation, and k_e is to be viewed as an average uptake rate.) Estimating the value of this uptake rate is one of our goals.
2. Binding and engulfment of an apoptotic cell by a macrophage is approximated as a single, fast and irreversible process. In reality, the process consists of multiple steps, with possibly reversible binding of the apoptotic cell to macrophage receptors followed (at some probability) by engulfment of the bound cell. However, *In vivo*, at body temperature, the lifetime of these complexes is very short, so that this stage is seldom observed, making this a reasonable assumption. Indeed, in order to observe such complexes, the temperature has to be lowered down to 4°C (Cocco and Ucker, 2001; O’Brien et al., 2002a,b). (At these low temperatures, the complexes of macrophages with bound apoptotic cells are relatively stable, owing to slow cytoskeletal rearrangement.)
3. We assume that engulfed apoptotic cells are digested and degraded in the macrophage sequentially (one by one) at rate k_d , and that this rate is roughly constant. (In our model, macrophages move from class i to class $i - 1$ at this rate). We refer to this as “saturated digestion” because when more internalised cells are present, it takes longer to complete the full digestion of the lot.
4. Death of macrophages (e.g. by apoptosis, typically on a time scale of days or weeks, Bellingan et al., 1996) is here neglected, since we focus on phagocytosis occurring on a time scale of hours. We also do not expect necrosis to contribute significantly on this time scale. The current experimental setting is not suitable for observing and quantifying macrophage death. Therefore, we cannot rule out some macrophage loss.

We refer to the model incorporating these assumptions as the **Basic Model** (Section 2.3). Later variants (Section 2.4) relax some assumptions, or incorporate others. One of our goals is to characterise which of the variants provides the best fit to the data.

2.3 Equations of the Basic Model

The simplest kinetic model proposed here is based on following the number of macrophages M_i , where $i = 1, 2, \dots$ is the number of ingested cells in macrophages of class i . The scheme of sequential stages is:



where k_e represents the combined rate of binding and engulfment, and k_d represents the rate of digestion. (See Table 1 for a summary of meanings and typical values of all symbols.) In this model, M_0 represents macrophages that have not yet engulfed, or that have already finished digesting apoptotic cells. The model equations track the “flow” into and out of each class. Flow toward higher classes (greater number of engulfed apoptotic cells) represents ingestion (proportional to the number of uningested apoptotic cells, A). Flow toward a lower class represents degradation of engulfed cells. In this model, apoptotic cells are taken up one at a time, and then digested sequentially, i.e. this is the “saturated digestion” case (see Assumption 3).

The set of differential equations for this model are:

$$\frac{dM_0}{dt} = -k_e M_0 A + k_d M_1 , \quad (2a)$$

$$\frac{dM_1}{dt} = k_e M_0 A - (k_d + k_e A) M_1 + k_d M_2 , \quad (2b)$$

$$\frac{dM_2}{dt} = k_e M_1 A - (k_d + k_e A) M_2 + k_d M_3 . \quad (2c)$$

The forms of the equations for macrophages in classes 1, 2, etc. are the same. In general, the i^{th} class satisfies an equation of the form:

$$\frac{dM_i}{dt} = k_e M_{i-1} A - (k_d + k_e A) M_i + k_d M_{i+1} . \quad (2d)$$

If a maximal number of ingested apoptotic cells (N) is considered, then the final equation for the macrophages containing N apoptotic cells is of the form:

$$\frac{dM_N}{dt} = k_e M_{N-1} A - k_d M_N . \quad (3)$$

For the purpose of simulations, we took $i = 1, \dots, N$, with the terminal value $N = 7$, unless indicated otherwise. We refer to N as the *macrophage capacity*.

Apoptotic cells are constantly being removed at a rate proportional to their density, A (with rate constant k_e). If there is no terminal macrophage class then:

$$\frac{dA}{dt} = -k_e A M , \text{ which gives } A(t) = A_0 e^{-k_e M t} , \quad (4a,b)$$

where A_0 is the initial density of apoptotic cells, and M is the total number of macrophages in all classes. If the terminal class of macrophages is M_N , then Eqn. (4) is replaced by:

$$\frac{dA}{dt} = -k_e A \sum_{i=0}^{N-1} M_i . \quad (5)$$

We used Eqn. (5) to fit data to the full model.

Initially, when the experiment starts, all macrophages are in the pre-phagocytic phase, M_0 , and none are in higher classes. The apoptotic cells are supplied at some fixed level A_0 . This determines the model initial conditions:

$$M_0(0) = M , M_i(0) = 0 \ (i = 1, \dots, N) , A(0) = A_0 . \quad (6)$$

The general behaviour of this model is that apoptotic cells decay as macrophages successively engulf them, first filling up the class M_1 , and then gradually filling up higher classes. The class M_0 will initially decrease, and later may increase once a significant fraction of the apoptotic cells have been digested.

Two common indices used to describe phagocytosis are the percent phagocytosis, Φ (the percent of macrophages that have visible engulfed cells), and the phagocytic index, I_Φ (the average number of engulfed cells per 100 macrophages), given by:

$$\Phi = \frac{100}{M} \sum_{i=1}^N M_i, \quad (7)$$

$$I_\Phi = \frac{100}{M} \sum_{i=1}^N iM_i. \quad (8)$$

The above set of equations comprises the basic model. Variants are discussed in the next section.

2.4 Model extensions

In the basic model we neglected possible activation of the macrophages from a resting state (Assumption 1). There is evidence, however, that stimulation of macrophages may affect the response and upregulate phagocytotic ability (Erwig et al., 1999; Licht et al., 2001; O’Brien et al., 2002b). We therefore considered a revised model in which the first engulfment occurs at a possibly lower rate than later engulfments, i.e. we relax Assumption 1. We call this first engulfment an “activation” step. Note that the term macrophage activation is used in many different ways, but that here it refers only to an upregulation of phagocytosis after initial uptake of an apoptotic cell. That is, we do not describe here differentiation of macrophages into antigen presenting cells (APC’s). Since inactivation probably occurs only after 24–48 hours, it seems unlikely to be a major effect over the time scale of interest here (i.e. over a few hours). Nevertheless, we investigated two extreme possibilities that activation is either rapidly reversible or fully irreversible (in variants I and II of the model).

A third variant of the basic model relaxes Assumption 3 that digestion is saturated. This assumption turns out to be important in our derivation of ball-park parameter estimates. We thus want to check the validity of this assumption, as we have no *a priori* knowledge about its accuracy. If, instead, the digestion machinery is unsaturated, (i.e. particles are digested in parallel, rather than one after another) then the rate of digestion per engulfed cell should be constant, and hence the rate of flow between classes should be proportional to the number i of ingested particles. Variant III explores this possibility.

Reversible macrophage activation step; model variant I

In model variant I, we explicitly include a reversible activation step: the rate of engulfment of the first apoptotic cell differs from the rates of subsequent ingestions. Upon full digestion, the macrophages revert to a non-activated state, and must again be activated on further encounter with cells to be engulfed. (See variant II for an irreversible version.) Model variant I is very similar to that of the basic model, but with the rate of activation, k_a , replacing the first forward rate constant k_e :



Equations for model variant I are then as before, but with the following changes to classes M_0, M_1 :

$$\frac{dM_0}{dt} = -k_a M_0 A + k_d M_1, \quad (10a)$$

$$\frac{dM_1}{dt} = k_a M_0 A - (k_d + k_e A) M_1 + k_d M_2. \quad (10b)$$

Irreversible activation of macrophages; model variant II

In model variant II, we assume that macrophages have an irreversible activation step, i.e. that they do not revert to their resting state on a time scale of a few hours. We define an additional class, M_u , representing the level of unactivated macrophages as shown below:



The equations for variant II are as before in Eqns. (2), but with new equations for M_u and M_1 :

$$\frac{dM_u}{dt} = -k_a M_u A, \quad (12a)$$

$$\frac{dM_1}{dt} = k_a M_u A + k_e M_0 A - (k_d + k_e A) M_1 + k_d M_2. \quad (12b)$$

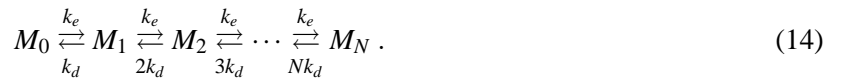
The macrophage mass balance is then:

$$M_u + \sum_{i=0}^N M_i = M. \quad (13)$$

We assume that initially, all macrophages are in the unactivated state, i.e. $M_u = M, M_i = 0$ for $i = 0, \dots, N$. Variants I and II differ only in the assumptions about reversibility of the resting state. (I assumes full reversibility, II assumes none.) While the actual situation is likely an intermediate case, we here only compare the two extremes, as current data are inconclusive. To obtain a more accurate description, either longer term data sets or experiments involving secondary meals are required. In these variants, the activation step delays the initial rise in M_1 . (Otherwise, the behaviour is similar.)

Unsaturated digestion; model variant III

Here we relax Assumption 3 that digestion is saturated. If, instead, digestion is unsaturated, its rate should be independent of the number of engulfed cells so that flux of macrophages from class i to class $i-1$ should be proportional to the rate k_d and to the number of cells to be digested, i . Then:



Here k_d is replaced everywhere by ik_d in the model, e.g.:

$$\frac{dM_i}{dt} = k_e M_{i-1} A - (ik_d + k_e A) M_i + (i+1)k_d M_{i+1}. \quad (15)$$

Unsaturated digestion could be combined with any of the above models, but here we discuss only the version that includes irreversible activation of macrophages (i.e. as in variant II). We refer to this combination as variant III, and find that it leads to a very bad fit. (This is discussed below.) Other combinations result in a worse fit, and are omitted here.

It is likely that the actual situation is an intermediate case, where digestion is optimally described by, for example, Michaelis-Menten kinetics. However, the current data are not well suited for determining kinetics at that level of detail. Further, our analysis suggests that the digestion saturates very rapidly. This justifies the simplification made here, pending availability of data that specifically address digestion. In this variant of digestion, we expect a much more rapid decay of all classes, since internalised particles are digested simultaneously, rather than one by one. Moreover, we expect relatively fewer macrophages in the higher classes.

2.5 Parameter fitting

Further on, we describe analysis of the models leading to easy parameter estimation. We also implemented full parameter fitting routines to the basic model ((2), (3), (5)), as well as to variants I, II, and III. To find the best-fit kinetic constants, k_e , k_d , and k_a , we used the Levenberg-Marquardt optimisation (Levenberg, 1944; Marquardt, 1963) of the freeware biochemical simulator program Gepasi (Mendes, 1993, 1997; Mendes and Kell, 1998). (The Levenberg-Marquardt optimisation method is a gradient descent technique, that combines steepest descent with a Newton method. Its advantages are rapid and robust convergence.) To arrive at parameter best-fit estimates, model predictions for the number of macrophages in the classes M_0, M_1, \dots, M_N were applied to data for all these observed classes over all times of observation. Previous studies have already showed a highly significant difference between Balb/c and NOD macrophage phagocytosis, albeit not by determining quantitative kinetic parameter values (O'Brien et al., 2002b). Moreover, the combined data for both mouse strains gives a very bad fit to any single model. (This is apparent in view of the huge difference in the phagocytosis in Figures 2 and 3; note the four-fold difference in scale in Figure 3.) We therefore present only fits which are done independently for Balb/c and NOD macrophages. The maximum number of visible engulfed apoptotic cells observed experimentally was $N = 7$. We tested the model for $N = 7$ as well as a higher value, $N = 12$, and found no difference in the predictions. In the experiments, cells have to be fixated and stained for counting, so no true time series are available. However, as described in Section 2.1, semi-independent time series were derived by mixing macrophages from different animals prior to seeding into wells.

We compared two data-fitting methods, concurrent and by replicate. By “concurrent” we mean a fit in which all data points of the 5 replicates are fit simultaneously, ignoring the fact that they are derived from different aliquots of macrophages. In fitting “by replicate” this distinction is preserved. We display results of both in this paper to make two important points, the relationship of the replicates, and the accuracy of our parameter estimates, as discussed below.

When a concurrent fitting is made to all data points simultaneously, any characteristics that are specific to distinct replicates may get lost. From the raw data itself, it was not clear whether replicates show distinct or identical trends, and we did not want to exclude this possibility *a priori*. Thus, we tested both methods, i.e. concurrent fitting to all the data points of each strain, as well as independent fittings to the time series that were composed by measurements on a specific replicate (i.e. based on the same initial mixture of macrophages). In our experiments, the animals are all genetically similar, and each curve represents the behaviour of macrophages pooled from many animals (see experimental methods), so we found little inter-experiment variation, which is reasonable. Later on, when searching for the most parsimonious description of the data, we compare whether taking the individual replicates into account significantly improves the

goodness-of-fit.

Concurrent data fitting allows us to calculate a confidence interval for the parameter values, based on the drop in the goodness-of-fit when each individual parameter is changed. A well-chosen concurrent change of more than one kinetic parameter, however, can lead to a much smaller drop in the goodness-of-fit. (In our data, this is due to the fact that when both engulfment and digestion rates are high, the fit is almost as good as when both are low.) Hence we expect this method to *de facto* underestimate the confidence interval. In contrast, fitting the data to the individual replicates allows for the calculation of a more ‘traditional’ standard deviation, since the outcome of the fittings can be considered to be five independent measurements of the same kinetic constant. However, since now, SD values are based on five values only (and, for the SD, do not take into account the huge amount of data), we expect to over-estimate the confidence interval. (This is why it is in general better to calculate SD values using raw data (Motulsky and Christopoulos, 2003).) Using both the fitting methods, therefore, allows us to both determine whether inter-experiment variation is significant and to assess the reliability of our parameter estimates.

2.6 Model selection

To determine which model best describes the observed phagocytosis, we used Akaike’s ‘An’ Information Criterion (*AIC*) (Akaike, 1973). A practical introduction to the usage of *AIC* to compare biological models can be found in Motulsky and Christopoulos (2003). *AIC* has been developed to determine which candidate model minimises the Kullback-Leibler divergence (a measure of ‘discrepancy’) between the true distribution and the model. Essentially, *AIC* maximises the probability that a candidate model generated the observed data by rewarding descriptive accuracy, while penalising an increase in the number of free parameters. *AIC* may perform poorly if there are too many parameters in relation to the size of the sample (Sugiura, 1978; Sakamoto et al., 1986). We therefore use a second order bias correction, recommended when the ratio of sample size to the number of parameters is smaller than 40 (as in our case). This small-sample adjustment has been derived by Sugiura (1978); Hurvich and Tsai (1989), and is called *AIC_c*. *AIC* and *AIC_c* converge at larger sample sizes.

AIC_c is defined as:

$$AIC_c = n \ln \left(\frac{SSE}{n} \right) + 2K + \frac{2K(K+1)}{n-K-1}, \quad (16)$$

where n is the number of observations, K the number of fitted parameters, and *SSE* the remaining sum of squared error after curve-fitting. The model with lowest *AIC_c* value is considered to be the best model. Since *AIC_c* adds a ‘penalty’ for each additional parameter, the most parsimonious description of the data is rewarded.

Differences in the *AIC_c* values can be used to calculate the likelihood that a given model best describes the data. An estimate of the relative likelihood L of model i , given the data is:

$$L(i|data) \propto e^{-0.5 \cdot \Delta_i(AIC_c)}, \quad (17)$$

where $\Delta_i(AIC_c) = (AIC_c)_i - \min(AIC_c)$, and the minimum is taken over all candidate models.

The relative model likelihoods are normalised (by dividing by the sum of the likelihoods of all models) to obtain the so-called Akaike weights w_i (see, e.g. Burnham and Anderson, 2002):

$$w_i = \frac{e^{-0.5 \cdot \Delta_i(AIC_c)}}{\sum_{j=1}^M e^{-0.5 \cdot \Delta_j(AIC_c)}}, \quad (18)$$

where M is the total number of models. The weight w_i can be interpreted as the probability that model i is the best model, given the data and the set of candidate models. Normalisation simply assures that $\sum_i w_i = 1$. The relative probabilities of any two candidate models i and j are then in proportion of the weights $w_i : w_j$. This relative probability does not change if a larger or smaller set of models is used in the comparison.

For example, in a simple comparison of two models, A and B , we define $\Delta(AIC_c) = |(AIC_c)_B - (AIC_c)_A|$, so that:

$$\text{probability that model } A \text{ is correct} = \frac{e^{-0.5 \cdot \Delta(AIC_c)}}{1 + e^{-0.5 \cdot \Delta(AIC_c)}}. \quad (19)$$

In this paper, we use the AIC_c method to ask whether, for a given mouse strain, the observed data are best described as separate, nonidentical trends or as a single uniform trend for the replicate experiments, and further, for the given strain, which of the model variants best fits the data. Note that describing R individual replicates with K parameters each is equivalent to a larger description (that can be considered as a distinct model) with a total of $R \times K$ parameters. For example, using the basic model, $K = 2$, and $R = 5$ experimental replicates per mouse strain, we end up with 10 fitted parameter values for each strain by the replicate fitting method. As discussed above, the AIC method allows us to compare all of these models simultaneously, as well as any two or more within the set.

3 Model analysis

In this section, we derive ball-park parameter estimates from simple features of the data such as initial rise-times, phagocytic index, and percent phagocytosis.

3.1 Basic model

We make the following observations about the basic model equations:

Initial rise phase

In the beginning of the experiment, when all macrophages are in their quiescent, or resting state, all classes M_i other than M_0 are zero. This means that the initial rise of class M_1 (or equivalently decay of class M_0) is given by:

$$\frac{dM_1}{dt} \approx k_e M_0 A, \text{ or, equivalently: } \frac{dM_0}{dt} \approx -k_e M_0 A. \quad (20a,b)$$

The constant k_e can be obtained from the ratio of the rate of change dM_1/dt to the product $M_0 A$ at time $t = 0$. Recall from the initial conditions that at time $t = 0$, $M_0(0) = M$ and $A(0) = A_0$, so that $M_0 A = M A_0$ is known. The change in the number of macrophages with zero or one internal particle (ΔM_0 and ΔM_1 , respectively) is measured over some time period (Δt). We can thus approximate the value of the rate constant k_e with the following rough estimate:

$$k_e \approx \left(\frac{\Delta M_1}{\Delta t} \Big|_{t=0} \right) \cdot \frac{1}{M A_0}, \quad (21a)$$

or, equivalently:

$$k_e \approx \left(\frac{-\Delta M_0}{\Delta t} \Big|_{t=0} \right) \cdot \frac{1}{M A_0}. \quad (21b)$$

This calculation for k_e approximates the instantaneous change, dM_1/dt , at time $t = 0$, with a change over some finite (possibly large) time span. However, this approximation provides a convenient, simple estimate of the rate of binding-engulfment. The estimate is improved if the first data point for M_0 and M_1 is close to the beginning of the experiment, a feature we incorporated in refining experimental design. If Δt is large, this method will underestimate the value of k_e . The underestimation is smaller when ΔM_0 is used instead of ΔM_1 , since, after a short time, only very few macrophages have returned from state M_1 to M_0 .

For example, using our experimental data to perform the estimate suggested above, leads to the following comparison: The density of empty macrophages M_0 for a typical Balb/c is observed to drop by 12% during the first 5 minutes of the experiment. This means that $\Delta M_0 = -0.12M = -2.4 \cdot 10^4 \text{ cell mL}^{-1}$. By comparison, for a typical NOD, M_0 drops by only 3% over the same time period (i.e. $\Delta M_0 = -0.6 \cdot 10^4 \text{ cell mL}^{-1}$). Thus,

$$\text{For Balb/c: } k_e = \frac{2.4 \cdot 10^4 \text{ cell mL}^{-1}}{\frac{1}{12} \text{ hour}} \cdot \frac{1}{2 \cdot 10^5 \text{ cell mL}^{-1} \cdot 10^6 \text{ cell mL}^{-1}} = 14.4 \cdot 10^{-7} \text{ mL cell}^{-1} \text{ hour}^{-1}, \quad (22a)$$

$$\text{For NOD: } k_e = \frac{0.6 \cdot 10^4 \text{ cell mL}^{-1}}{\frac{1}{12} \text{ hour}} \cdot \frac{1}{2 \cdot 10^5 \text{ cell mL}^{-1} \cdot 10^6 \text{ cell mL}^{-1}} = 3.6 \cdot 10^{-7} \text{ mL cell}^{-1} \text{ hour}^{-1}. \quad (22b)$$

A comparison of these basic estimates clearly shows that the engulfment rate k_e of the NOD macrophages is much lower than the rate of the Balb/c macrophages. This could (partly) explain the reduced phagocytosis that was observed by O'Brien et al. (2002b,a).

Ratios of sizes of successive classes

After some time (circa 1 hour), the changes in relative sizes of the various classes slows down, and a quasi-steady state (QSS) is approximately established. (We discuss the validity of this QSS assumption in Section 4.4.) Then:

$$0 \approx -k_e M_0 A + k_d M_1, \quad (23a)$$

$$0 \approx k_e M_0 A - (k_d + k_e A) M_1 + k_d M_2, \quad (23b)$$

$$0 \approx k_e M_1 A - (k_d + k_e A) M_2 + k_d M_3, \text{ etc.} \quad (23c)$$

Sequentially solving the equations, we obtain approximate relationships between successive classes:

$$M_1 = \left(\frac{k_e A}{k_d} \right) M_0, M_2 = \left(\frac{k_e A}{k_d} \right) M_1, \dots, M_{i+1} = \left(\frac{k_e A}{k_d} \right) M_i, \text{ etc.} \quad (24)$$

We define λ by:

$$\lambda = \frac{k_e A}{k_d}. \quad (25)$$

Then :

$$M_{i+1} = \lambda M_i. \quad (26)$$

This implies that when A changes slowly, ratios of the successive classes also change slowly. If A is known (either from direct measurements, or from Eqns. (4) and (21)), then the parameter λ can be used to obtain the ratio k_e/k_d . We can then find k_d , using the independent estimate of k_e obtained from the initial rise phase. That is:

$$k_d = \frac{k_e A}{\lambda} = \frac{k_e A M_i}{M_{i+1}}. \quad (27)$$

It follows from Eqn. (26) that M_i is related to M_0 exponentially:

$$M_i = \lambda^i M_0 \quad (28)$$

(see, e.g. Edelstein-Keshet, 1988). This has some further implications. First, note that the total number of macrophages, $M = \sum M_i$, is related to M_0 via a geometric series:

$$M = M_0 + M_1 + M_2 + \dots = M_0 (1 + \lambda + \lambda^2 + \dots) = M_0 \sum_i \lambda^i. \quad (29)$$

For the biological range of values of the parameters, typically $\lambda \ll 1$, implying that M_i decays exponentially with i . The sum of the (finite) geometric series with N terms (i.e. assuming a maximal class, M_N), is:

$$M = M_0 \frac{\lambda^{N+1} - 1}{\lambda - 1}. \quad (30)$$

When the value of $\lambda < 1$ and N is sufficiently large, as in our case, the finite sum can be well approximated by the infinite sum ($1 + \lambda + \lambda^2 + \dots = 1/(1 - \lambda)$). (The formula is simpler and the value of N is then not needed, i.e. we do not have to specify the maximal capacity of a macrophage.) Then:

$$M \approx M_0 \frac{1}{1 - \lambda}, \quad (31)$$

from which we obtain the estimate:

$$k_d = \frac{k_e M A}{M - M_0}. \quad (32)$$

This provides an alternate estimate of the parameter k_d .

Aggregate phagocytic parameters

Using the basic model, we can link aggregate indices such as percent phagocytosis and phagocytic index to kinetic parameters of the model. As above, we assume that these indices are determined at times when the QSS approximation is reasonable. Then the percent phagocytosis is:

$$\Phi = \frac{100}{M} \sum_{i=1}^N M_i \approx \frac{100}{M} M_0 \frac{\lambda}{1 - \lambda} = 100 \lambda. \quad (33)$$

Further, using the previous k_e values, this implies that k_d is:

$$k_d = \frac{100 k_e A}{\Phi}. \quad (34)$$

This equation is equivalent to Eqn. (32). The phagocytic index is:

$$I_\Phi = \frac{100}{M} \sum_{i=1}^N i M_i = \frac{100}{M} M_0 \sum_{i=1}^N i \lambda^i \approx \frac{100}{M} M_0 \frac{\lambda}{(1 - \lambda)^2} = 100 \frac{\lambda}{(1 - \lambda)^2}. \quad (35)$$

The latter result follows readily from the observation that $\lambda < 1$ and the series converges, so that:

$$\sum_i i \lambda^i = \lambda \frac{d}{d\lambda} \left(\sum_i \lambda^i \right) = \lambda \frac{d}{d\lambda} \left(\frac{1}{1 - \lambda} \right) = \frac{\lambda}{(1 - \lambda)^2}. \quad (36)$$

This provides yet another estimate of the parameter k_d . From Eqn. (35), we obtain:

$$k_d = \left(\frac{100}{I_\Phi} + 1 \right) k_e A. \quad (37)$$

3.2 Model variant I

Analysis of this variant is similar, with the following minor changes:

The initial rise time is used to find the activation rate, k_a (the rate of the first engulfment step), i.e.:

$$k_a \approx \left(\frac{\Delta M_1}{\Delta t} \Big|_{t=0} \right) \cdot \frac{1}{MA_0}, \text{ or, equivalently: } k_a \approx \left(\frac{-\Delta M_0}{\Delta t} \Big|_{t=0} \right) \cdot \frac{1}{MA_0}. \quad (38a,b)$$

The engulfment rate, k_e , is found from data for higher classes. For example, we select time points $t_1 < t < t_2$ such that M_2 increases significantly from very low levels over this interval. Then, we find k_e from the rise time of M_2 . That is, from Eqn. (2c):

$$k_e \approx \left(\frac{\Delta M_2}{\Delta t} \Big|_{t=t_1} \right) \cdot \frac{1}{M_1(t)A(t)}, \quad (39)$$

where $\Delta t = (t_2 - t_1)$, ΔM_2 is the change in M_2 , and $M_1(t)$, $A(t)$ are averaged over the given interval. When not measured, an estimate of the concurrent level of A can be obtained using the connections between the different classes, as shown below.

The connection between the first two classes with QSS approximation is given by:

$$M_1 = \lambda_a M_0, \text{ where } \lambda_a = \left(\frac{k_a A}{k_d} \right). \quad (40a,b)$$

Activation affects only the first two classes, so all other classes are as before, i.e. $M_1 = \lambda_a M_0$, and $M_{i+1} = \lambda M_i$, for all other values of i . The ratio M_1/M_2 yields λ_a , and all other ratios M_{i+1}/M_i produce λ . Further, k_e can be found even if A is not measured, since $k_a/k_e = \lambda_a/\lambda$, is independent of A . Hence:

$$k_e = \frac{k_a \lambda}{\lambda_a}. \quad (41)$$

The above also implies that $M_i = \lambda_a \lambda^{i-1} M_0$, so that the total number of macrophages, M , is related to the initial class M_0 by:

$$M \approx M_0 \left(\frac{1 - \lambda + \lambda_a}{1 - \lambda} \right), \text{ or, equivalently: } M_0 \approx M \left(\frac{1 - \lambda}{1 - \lambda + \lambda_a} \right). \quad (42)$$

The equation that governs the depletion of apoptotic cells is now:

$$\frac{dA}{dt} = -k_a M_0 A - k_e \sum_{i=1}^{N-1} M_i. \quad (43)$$

During the initial phase, the dynamics are approximately:

$$\frac{dA}{dt} \approx -k_a M A, \text{ which gives: } A(t) = A_0 e^{-k_a M t}; \quad (44a,b)$$

later on, when M_i is on QSS, the dynamics can be described by:

$$\frac{dA}{dt} \approx \left(-k_a \frac{1 - \lambda}{1 - \lambda + \lambda_a} - k_e \frac{\lambda_a}{1 - \lambda + \lambda_a} \right) M A. \quad (45)$$

The percent phagocytosis, Φ , is now given by:

$$\Phi = \frac{100}{M} \sum_{i=1}^N M_i \approx \frac{100}{M} M_0 \frac{\lambda_a}{1-\lambda} = 100 \frac{\lambda_a}{1-\lambda+\lambda_a}. \quad (46)$$

The phagocytic index, I_Φ , can also be expressed in terms of the same parameters:

$$I_\Phi = \frac{100}{M} \sum_{i=1}^N i M_i \approx 100 \frac{\lambda_a}{(1-\lambda+\lambda_a)(1-\lambda)}. \quad (47)$$

Using Eqns. (46) and (47), we can calculate λ and λ_a directly from Φ and I_Φ :

$$\lambda_a = \frac{\Phi^2}{I_\Phi(100-\Phi)}, \quad (48a)$$

$$\lambda = \frac{I_\Phi - \Phi}{I_\Phi}. \quad (48b)$$

Using the fact that $k_a/k_e = \lambda_a/\lambda$, we then obtain another estimate for k_e :

$$k_e = \frac{k_a \lambda}{\lambda_a} = \frac{k_a (I_\Phi - \Phi)(100 - \Phi)}{\Phi^2}. \quad (49)$$

Neither of the above two independent estimates for k_e requires an *a priori* value for A (but finding k_d does). Using these estimates, we find, for example, that in Balb/c k_e is 1.5 to 2 times larger than k_a . In NOD, however, the engulfment rate does not seem to increase.

4 Phagocytotic ability

We here use the basic estimates of Section 3 and full parameter fits to compare the phagocytotic parameters of NOD and Balb/c mice. We also test which model variant optimally fits the data.

4.1 Ball park estimates

The ball park estimates are based on elementary properties of the data and aggregate quantities (such as Φ and I_Φ). An advantage is that fewer data points are needed, so that an investigator could compare values of parameters with a less onerous experiment.

Table 2 summarises ball park estimates for Balb/c and NOD phagocytosis parameters. Even these crude estimates clearly indicate that NOD and Balb/c macrophages have quantitatively distinct rates of activation and engulfment of apoptotic cells. We find similar rates of digestion, k_d , but the rate of engulfment, k_e , is 4 times higher for Balb/c than for NOD macrophages. Differences between the mouse types become even more apparent considering the model variant with a possible activation step. The rate of activation (and first engulfment), k_a , is still 4 times larger for the Balb/c mice. However, after activation Balb/c macrophages engulf even faster, while macrophages of NOD mice lack this activation step. Consequently, the rate of engulfment after activation, k_e , is 7 times greater for Balb/c macrophages than for NOD macrophages.

4.2 Parameter fitting

As described in Section 2.5, we carried out a full parameter fitting to the dynamical models, using both concurrent fitting and fitting to the individual replicates (see Section 2.5). We display results of both fitting methods, to emphasise our findings on whether inter-experiment variation is significant and to assess the accuracy of the parameter estimates. The best-fit parameters obtained for the respective models are given in Table 3 for the concurrent fitting method, and in Table 4 for the replicate fitting method. Parameter fits were found for (1) The basic model; (2) model variant I, with reversible activation; (3) model variant II, with irreversible activation and macrophage capacity $N = 7$; (4) model variant II, but with macrophage capacity $N = 12$; (5) model variant III, with unsaturated digestion. We make the following observations:

Replicate vs. concurrent fit: Table 3 and Table 4 demonstrate that replicate and concurrent fitting give essentially the same estimates for the kinetic parameters. This may stem from genetic homogeneity of the NOD mice, as well as the fact that mixing of samples from multiple animals dilutes any inter-animal variability.

Ball-park estimates versus full-model fits: Comparing Table 2 with Tables 3 and 4, we find reasonably good agreement, differing by less than 50%. Early time points are essential. In older experiments, where $t_1=30$ min, rise time was grossly misrepresented, leading to discrepancies by factors of 2-5 between ball-park estimates and full parameter fits.

4.3 Model selection and comparison

To select the models that give the best description of the observed phagocytosis, we used the corrected Akaike's Information Criterion AIC_c , and calculated the likelihood that the given model is best, using the Akaike weights w_i . A summary of the results of the AIC_c calculation is given in Table 5 for Balb/c followed by NOD mouse strains. We also refer to Tables 2 and 3, from which the following results are obtained.

- For NOD macrophages, the basic model (with concurrent fit) gives the best description of phagocytosis (with a likelihood of $\approx 46\%$). Recall that in Tables 2 and 3 there is no significant difference in NOD engulfment before and after activation. Thus, it is reasonable that for NOD the most parsimonious description is the basic model *without* activation. This implies that, most likely, the NOD macrophages do not undergo an activation step during the course of the experiment.
- In Balb/c, model Variant I (fit concurrently) is the best description of phagocytosis by Balb/c macrophages (with a likelihood of $\approx 38\%$). This model is nearly three times more likely to be the right description than the basic model with distinct replicate behaviour ($\approx 14\%$). Indeed, a distinct rate of Balb/c activation and a much faster subsequent rate of Balb/c engulfment was found (Tables 2 and 3). Thus, it is reasonable that a model with an activation step best describes the Balb/c data.
- When further comparing the various activation-step models, we find that in Balb/c macrophages, reversible activation is 1.5 times more likely than irreversible activation (with weights ratios for variant I vs II of roughly 38 : 25 with $N = 7$, and 38 : 21 for $N = 12$). For NOD macrophages, there is a small but non-negligible probability that some very low level of activation occurs, but, then, reversible and irreversible activation is equally likely (15 -18%). Such differences are quite small, so that the current experiments do not definitively indicate whether macrophage activation is reversible or irreversible. We expect that macrophages slowly return to rest state after digesting their full apoptotic meal, but, as the time scale is much longer, the current data cannot quantify this reversion.

- Variant III (unsaturated digestion) results in very bad fits (probabilities close to 0), indicating that digestion saturates very rapidly. This means that the rate of digestion is similar for macrophages containing one or many apoptotic cells, i.e. k_d must be roughly constant at all stages. More extensive studies on the decay dynamics of engulfed apoptotic cells, however, could lead to a more detailed description of the degradation process.
- Tables 3 and 5 indicate that varying the macrophage capacity (from $N=7$ to 12) has very little influence on the results, so taking $N = 7$ is reasonable. Note, however, that since $\lambda \ll 1$, the probability of observing macrophages with 8 or more engulfed apoptotic cells is extremely small. The experiments do not allow us to determine the value of the true macrophage capacity; to do this, we would need experiments with much higher densities of apoptotic cells.
- Based on the AIC_c comparison of concurrent versus replicate fitting, it is very unlikely that the individual replicates truly differ in their kinetic parameters. For NOD mice, the reduction in the SSE obtained by splitting the data up into individual replicates is so marginal, that the likelihood that one of the replicate models best describes the observed data is smaller than 0.1%. For the more genetically variable Balb/c mice, it is more likely that the reduction in SSE truly represents variation between replicates. (Note also the larger value of the standard deviation for Balb/c parameter fits in Tables 2 and 3). The possibility that Balb/c macrophages lack the activation step, but simply have a higher level of inter-mouse variation, has a likelihood of 14%, and so, should not be discounted. (However, it is nearly three times more likely that the experimental replicates are essentially similar and that the activation step is real.)
- From Tables 4 and 3, we see that there is a highly significant difference in the values of k_e for Balb/c and NOD macrophages, regardless of the model or method used to fit parameters. The Balb/c macrophages engulf apoptotic cells 4-5 times faster than the NOD macrophages. Furthermore, these tables show that the engulfment rate after activation increases significantly in Balb/c (by 1/2 to 2-fold) but not in NOD macrophages. Finally, the digestion rates k_d are not significantly different in the two mouse strains. (Even if the differences in k_d for the strains and the difference between k_e and k_d in NOD mice are statistically significant, the biological relevance of such small differences would be questionable. Rigorously establishing such statistical significance of such closely comparable values would be tricky, in view of the many models being compared and different methods used to determine the means and standard deviations.)

In summary, these remarks strongly suggest that NOD macrophages suffer from a reduced activation and engulfment rate, but not a reduced digestion rate. After their first engulfment, Balb/c macrophages engulf more than 5 times faster than NOD macrophages (while the digestion rate, k_d , hardly differs). The rate of digestion is similar for macrophages containing one or many apoptotic cells, meaning that the degradation machinery always seems to function in the saturated regime.

4.4 Model dynamics

Figure 2 compares experimental data (points) with all model variants for the two mouse types. The predicted dynamics (superimposed curves) follow the observed data very closely. Because of the very small sampling sizes of the higher classes, only M_0 up to M_3 are shown. We show the concurrent fitting (found to be better than fitting to individual replicates, not shown). Only variant III (unsaturated digestion) clearly cannot account for the observed dynamics. For Balb/c, the basic model also falls short by highly overestimating

early phagocytosis, yet another indication that macrophage activation is important in Balb/c. For both mouse types, phagocytosis is underestimated at the latest time point. This is also apparent in Figure 3, where a similar data-model comparison is made for the indices, Φ and I_Φ : at the latest time point, both Φ and I_Φ are underestimated. (Agreement at earlier times is encouraging, in view of the fact that the models have not been fitted to the measured Φ and I_Φ .)

Figure 4 shows the time course behaviour of macrophage classes and the predicted level of apoptotic cells, $A(t)$, according to the basic model and variant I. (Recall that the level of apoptotic cells was not experimentally measurable, and is one of the predictions of the model.) Both models predict a huge drop in $A(t)$ (by 50% for NOD and 90% for Balb/c after 8 hours) which leads to a resulting drop in phagocytosis at the latest time points. A more gradual decline of $A(t)$, (or a reduced searching efficiency of macrophages at lower feeding densities, not considered here) could account for underestimation of the Φ and I_Φ after 8 hours.

Figure 5 shows populations over time according to model variants II and III (reversible activation and unsaturated digestion, respectively). We find a two-fold difference in the level of apoptotic cells predicted by variant I versus variant II. Figure 4 and 5 therefore indicate the considerable importance of experimentally quantifying the level of apoptotic cells, $A(t)$, not only for engulfment efficiency, but also for determining whether macrophage activation is reversible on a relatively short time scale.

Figure 6 shows the dynamics of λ for the basic model (Eqn. (25)) and λ_a for model variant I with reversible activation (Eqn. (40b)), for Balb/c and NOD mice, compared with the QSS estimates of these parameters. This verifies that a QSS approximation becomes reasonable (i.e. within 50%) after about 1 hour; truly comparable values (i.e. within 10–20%) are found only after 2-3 hours. The ball park estimates based on these QSS assumptions therefore only take into account data points that are ≥ 1 hour.

5 Discussion and Conclusions

In this paper, we have analysed a number of models for macrophage engulfment and digestion of apoptotic cells. Experimental data in which successive macrophage classes were followed was then used to fit parameter values. We used the Akaike criterion to select which of a number of model variants gave the best description of the process. Several authors have also considered models in which macrophages with $1, 2, \dots, N$ internalised particles are followed. Gammack et al. (2004) considered macrophages engulfing *Mycobacterium tuberculosis*, in an investigation of the dynamics of the infection, with no detailed consideration of phagocytosis; they assumed that macrophages engulf up to $N=2$ bacterial cells only.

Analysing phagocytosis in macrophages from Balb/c and NOD mice reveals an NOD impairment in activation and engulfment, but not in digestion of apoptotic cells. Other insights include the following:

- In Balb/c macrophages, the rate of activation, k_a , is 1.5 to 2 times slower than the subsequent rate of engulfment, k_e . In NOD mice, no such difference is detected during our experiments. This indicates that a good description of normal phagocytosis should take into account a delay in the first step.
- We have interpreted the absence of activation step in the NOD macrophages to indicate a possibly pathological defect in macrophage function in these mice. A possibility remains that in the autoimmune-prone NOD mice, macrophages may have already been exposed to apoptotic cells that caused activation. In that case, NOD macrophages might be pre-activated, (unlike Balb/c) before the experiment begins. Nevertheless, their maximal rate of engulfment is 4-5 times lower than that of the Balb/c macrophages, which constitutes a significant difference.

- Due to technical issues, the decaying number of apoptotic cells, $A(t)$ could not be measured over the time course of our experiments, so model fits were used to predict $A(t)$. Over about 8 hours, these predict that A drops by $\pm 90\%$ versus $\pm 50\%$ for, respectively, Balb/c versus NOD macrophages. This difference, and the disparity between predicted $A(t)$ for distinct model variants, indicates the importance of experiments that allow $A(t)$ to be observed. Such data could also help to distinguish between reversible and irreversible activation.
- No maximal ‘macrophage capacity’ has to be assumed, since $N = 7$ or 12 are indistinguishable in the fits. While we cannot here quantify a maximal capacity, under our experimental conditions, we rarely observe a large number of visible engulfed apoptotic cells inside one macrophage. Our modelling shows that this is expected in general (and that it does not depend on a ‘macrophage capacity’): the ‘macrophage capacity’ is essentially irrelevant for understanding and quantifying the process of phagocytosis. Moreover, there is also no indication that the engulfment rate decreases with increasing numbers of engulfed cells: ratios of successive macrophage classes are virtually constant beyond the early activation step, which suggests that the parameter k_e is the same for all higher classes. (Note that implementation of a phagocytic ceiling or decreasing engulfment rates as was done in, for example, Gammack et al. (2004) and Tran et al. (1995), is not needed to explain the very low levels of macrophages in higher classes.)

Our derivations of ball park estimates for the kinetic phagocytosis parameters are of broader applicability. The advantage is the relatively easy calculations (based on common phagocytosis indices), and the need for fewer data points. However, there are limitations. Many ball park estimates assume a QSS which does only moderately well after one hour; after more than three hours the QSS assumption still makes an error of 10–20%.

The ball park values underestimate the engulfment rate k_e and activation rate k_a , because return to the rest state is ignored. This is especially true when no early data points are available. Underestimating k_e has a strong effect on the estimate of the rate of digestion, k_d , derived from it. So early measurements are important for correctly quantifying k_d as well as k_e . Further, differences between engulfment rates are less pronounced in the ball park estimates, which moreover could mask potential differences in k_d .

This argues for using full model fits when early data are unavailable. Moreover, since biological data are highly variable, relying on rise times based on a small subset of the data leads to larger errors than a full model fit. Full model fits, however, are also sensitive to missing early data points, especially when the abundance of apoptotic cells, A , is not measured. Under such settings, one finds a ‘ridge’ of very good data fits, with many different combinations of k_e and k_d leading to almost exactly the same quality-of-fit. At the same time, some of the ball park estimates depend on A . For example, in some cases k_d cannot be found when this value is not known.

Taken together, our study shows the importance of both early and late data points, as well as observations of the decreasing level of apoptotic cells. An alternative to measuring $A(t)$, however, could be a strategy of continually adding apoptotic cells to the medium during the experiment, to avoid depletion of A . Ideally, a short term study like ours (up to 8 hours) should be combined with a long-term study (up to 2–3 days) to quantify gradual changes in the activation state. This might also resolve contradictions in the literature about whether or not it is harder to reactivate macrophages after they have returned to a resting state (Erwig et al., 1999; Licht et al., 2001; O’Brien et al., 2002b).

To explain *in vitro* macrophage phagocytosis data, our models assumed (1) engulfment of an apoptotic cell; (2) an activation step causing accelerated subsequent engulfments; and (3) digestion. The models are based on reasonable approximations (given the current data and level of detail) such as mass-action kinetics,

a single irreversible process of binding and engulfment, and no phagocytotic ceiling. The rate of engulfment (in $\text{mL cell}^{-1} \text{h}^{-1}$) was found to be 4 (for NOD) vs. 12 (for Balb/c). The rate of digestion is 1 h^{-1} for both types. NOD macrophages have no visible activation step, but for Balb/c mice, the engulfment rate increased to around $23 \text{ mL cell}^{-1} \text{ h}^{-1}$, i.e. 3–6 times greater than the corresponding NOD mouse values. This means that Balb/c macrophages are significantly more active.

Our analysis strongly indicates that NOD macrophages have defective engulfment. Furthermore, these macrophages do not show an acceleration of engulfment after their first encounter with apoptotic cells (i.e. we do not observe an “activation step”). We could speculate that this defect could be due either to defective receptors associated with phagocytosis, or to lower macrophage motility that would reduce rates of encounter with apoptotic cells. Another explanation for the missing activation step could be that it had occurred *in vivo* prior to harvesting of these cells. However, even if this is the case, the highest rates of engulfment of the NOD macrophages are much lower than their Balb/c counterparts.

Defective engulfment implies that clearance of apoptotic cells is reduced in NOD mice. Consequently, levels of apoptotic β -cells remaining in the tissue should be much higher in NOD than in Balb/c mice. This idea could give rise to two interrelated consequences. On one hand, necrosis of such apoptotic β -cells may give rise to local inflammatory responses that escalate and eventually lead to insulinitis and diabetes. On the other hand, the self-antigen that is not promptly removed could lead to presentation by dendritic cells that activate cytotoxic T cells. These, in turn, could selectively target and kill β -cells, causing further pathogenesis and autoimmunity. Taken together, these ideas may explain the predisposition of NOD mice to autoimmune diabetes. Future modelling efforts will aim to assess such hypotheses in greater detail.

Acknowledgements: We are grateful to Bronwyn O’Brien for discussions and initial experimental data (not here reported). We also thank Xuan Geng for assisting M.K. with the experimental set-up. The modelling research was supported by the Mathematics of Information Technology and Complex Systems (MITACS) of Canada. Experimental work was supported by the Canadian Institutes for Health Research, and the Juvenile Diabetes Research Foundation.

References

- H. Akaike. Information theory as an extension of the maximum likelihood principle. In B. N. Petrov and F. Csaki, editors, *Second International Symposium on Information Theory*, pages 267–281. Akademiai Kiado, Budapest, 1973.
- D. G. Alleva, R. P. Pavlovich, C. Grant, S. B. Kaser, and D. I. Beller. Aberrant macrophage cytokine production is a conserved feature among autoimmune-prone mouse strains: elevated interleukin (IL)-12 and an imbalance in tumor necrosis factor-alpha and IL-10 define a unique cytokine profile in macrophages from young nonobese diabetic mice. *Diabetes*, 49:1106–1115, 2000.
- G. J. Bellingan, H. Caldwell, S. E. M. Howie, I. Dransfield, and C. Haslett. In vivo fate of the inflammatory macrophage during the resolution of inflammation: inflammatory macrophages do not die locally, but emigrate to the draining lymph nodes. *J. Immunol.*, 157:2577–2585, 1996.
- K. P. Burnham and D. R. Anderson. *Model selection and multimodel inference: a practical information-theoretic approach*. Springer-Verlag, New York, 2002.
- R. E. Cocco and D. S. Ucker. Distinct modes of macrophage recognition for apoptotic and necrotic cells are not specified exclusively by phosphatidylserine exposure. *Mol. Biol. Cell*, 12:919–930, 2001.

- L. Edelstein-Keshet. *Mathematical Models In Biology*, chapter 1. Random House, New York, 1988.
- L.-P. Erwig, S. Gordon, G. M. Walsh, and A. J. Rees. Previous uptake of apoptotic neutrophils or ligation of integrin receptors downmodulates the ability of macrophages to ingest apoptotic neutrophils. *Blood*, 93: 1406–1412, 1999.
- D. Gammack, C. R. Doering, and D. E. Kirschner. Macrophage response to *mycobacterium tuberculosis* infection. *J. Math. Biol.*, 48(2):218–242, February 2004.
- H. M. Georgiou, D. Constantinou, and T. E. Mandel. Prevention of autoimmunity in nonobese diabetic (NOD) mice by neonatal transfer of allogeneic thymic macrophages. *Autoimmunity*, 21:89–97, 1995.
- S. Gordon. The role of the macrophage in immune regulation. *Res. Immunol.*, 149:685–688, 1998.
- C. M. Hurvich and C.-L. Tsai. Regression and time series model selection in small samples. *Biometrika*, 76:297–307, 1989.
- H.-S. Jun, C.-S. Yoon, L. Zbytnuik, N. Van Rooijen, and J.-W. Yoon. The role of macrophages in T cell-mediated autoimmune diabetes in nonobese diabetic mice. *J. Exp. Med.*, 189:347–358, 1999.
- K. Levenberg. A method for the solution of certain nonlinear problems in least squares. *Quart. Appl. Math.*, 2:164–168, 1944.
- R. Licht, C. W. M. Jacobs, W. J. M. Tax, and J. H. M. Berden. No constitutive defect in phagocytosis of apoptotic cells by resident peritoneal macrophages from pre-morbid lupus mice. *Lupus*, 10:102–107, 2001.
- D. W. Marquardt. An algorithm for least squares estimation of nonlinear parameters. *SIAM J.*, 11:431–441, 1963.
- D. Mathis, L. Vence, and C. Benoist. β -Cell death during progression to diabetes. *Nature*, 414(6865): 792–798, December 2001.
- P. Mendes. GEPASI: a software package for modelling the dynamics, steady states and control of biochemical and other systems. *Comput. Appl. Biosci.*, 9:563–571, 1993.
- P. Mendes. Biochemistry by numbers: simulation of biochemical pathways with gepasi 3. *Trends Biochem. Sci.*, 22:361–363, 1997.
- P. Mendes and D. B. Kell. Non-linear optimization of biochemical pathways: applications to metabolic engineering and parameter estimation. *Bioinformatics*, 14:869–883, 1998.
- H. J. Motulsky and A. Christopoulos. *Fitting models to biological data using linear and nonlinear regression: a practical guide to curve fitting*. GraphPad Software Inc., San Diego CA, 2003.
- B. A. O’Brien, W. E. Fieldus, C. J. Field, and D. T. Finegood. Clearance of apoptotic beta-cells is reduced in neonatal autoimmune diabetes-prone rats. *Cell Death. Differ.*, 9:457–464, 2002a.
- B. A. O’Brien, Y. Huang, X. Geng, J. P. Dutz, and D. T. Finegood. Phagocytosis of apoptotic cells by macrophages from NOD mice is reduced. *Diabetes*, 51:2481–2488, 2002b.

- Y. Sakamoto, M. Ishiguro, and G. Kitagawa. *Akaike information criterion statistics*. KTK Scientific Publishers, Tokyo, 1986.
- A. Shimada, I. Takei, T. Maruyama, A. Kasuga, T. Kasatani, K. Watanabe, Y. Asaba, T. Ishii, T. Tadakuma, S. Habu, et al. Acceleration of diabetes in young NOD mice with peritoneal macrophages. *Diabetes Res. Clin. Pract.*, 24:69–76, 1994.
- N. Sugiura. Further analysis of the data by Akaike's information criterion and the finite corrections. *Commun. Statist. Theory Meth.*, A7:13–26, 1978.
- C. L. Tran, A. D. Jones, and K. Donaldson. Mathematical model of phagocytosis and inflammation after the inhalation of quartz at different concentrations. *Scand. J. Work. Environ. Health.*, 21:50–54, 1995.
- J. D. Trudeau, J. P. Dutz, E. Arany, D. J. Hill, W. E. Fieldus, and D. T. Finegood. Neonatal beta-cell apoptosis: a trigger for autoimmune diabetes? *Diabetes*, 49(1):1–7, January 2000.

Tables

Table 1: Model variables and parameters. The objective is to estimate k_d , k_e and k_a using the observed time courses of M_i , Φ and I_Φ .

Symbol	Meaning	Range of values
<u>Variables</u>		
A	density of apoptotic cells	10^5 – 10^6 cell mL ⁻¹
M_i	density of macrophages with i engulfed apoptotic cells	0 – $2 \cdot 10^5$ cell mL ⁻¹
M_u	density of unactivated macrophages	$5 \cdot 10^4$ – $2 \cdot 10^5$ cell mL ⁻¹
Φ	% phagocytosis (fraction of all macrophages containing at least one engulfed apoptotic cell)	0 – 60
I_Φ	phagocytic index (number of engulfed apoptotic cells per 100 macrophages)	0 – 175
<u>Parameters</u>		
N	maximum number of engulfed apoptotic cells observed within a single macrophage	7
M	total density of macrophages	$2 \cdot 10^5$ cell mL ⁻¹ ^[a]
A_0	initial density of apoptotic cells	10^6 cell mL ⁻¹ ^[a]
k_e	rate by which macrophages engulf apoptotic cells	10^{-7} – 10^{-5} mL cell ⁻¹ hour ⁻¹ ^[b]
k_a	rate by which unactivated macrophages engulf apoptotic cells and consequently become activated	10^{-7} – $2 \cdot 10^{-6}$ mL cell ⁻¹ hour ⁻¹ ^[b]
k_d	rate by which apoptotic cells are digested	0.4 – 2 hour ⁻¹ ^[b]

^[a] M and A_0 were estimated as follows: the number of adherent macrophages per well $\approx 10^5$ (well-to-well variation not quantified); the number of apoptotic thymocytes added to each well $\approx 5 \times 10^5$ (adjusted to achieve the 5:1 ratio); and the well volume ≈ 0.5 mL.

^[b] These parameters were estimated by methods described in this paper.

Table 2: Ball park estimates of the kinetic parameters for engulfment and digestion of apoptotic cells by macrophages. We used the initial rise time, the ratios between the different classes, the % phagocytosis, Φ , and the phagocytic index, I_Φ , to estimate these quantities. For estimates that require the quasi-steady state (QSS) assumption, time points ≥ 1 hour are used. The values are given as mean \pm standard deviation (SD).

parameter	based on Eqn.	# measurements	Balb/c	NOD
basic model				
k_e (10^{-7} mL cell $^{-1}$ h $^{-1}$)	(21a)	4	12.4 \pm 7.4	3.1 \pm 2.5
k_e (10^{-7} mL cell $^{-1}$ h $^{-1}$)	(21b)	4	14.9 \pm 10.1	3.2 \pm 2.5
k_d (h $^{-1}$)	(27)	182	1.18 \pm 1.39	1.02 \pm 1.01
k_d (h $^{-1}$)	(32)	26	1.38 \pm 1.49	1.06 \pm 0.55
k_d (h $^{-1}$)	(37)	26	1.31 \pm 1.35	1.07 \pm 0.52
model variant I				
k_a (10^{-7} mL cell $^{-1}$ h $^{-1}$)	(38b)	4	14.9 \pm 10.1	3.2 \pm 2.5
k_e (10^{-7} mL cell $^{-1}$ h $^{-1}$)	(41)	26	26.3 \pm 12.4	3.7 \pm 2.0
k_e (10^{-7} mL cell $^{-1}$ h $^{-1}$)	(49)	26	19.3 \pm 8.8	3.0 \pm 1.1

Table 3: Best fits for the kinetic parameters describing engulfment, activation and digestion of apoptotic cells by macrophages for the various models. The values are given as mean \pm SD. Each parameter estimate is based on concurrent data fitting to 45 measurements.

parameter	Balb/c	NOD
basic model		
k_e (10^{-7} mL cell $^{-1}$ h $^{-1}$)	12.1 \pm 0.33	4.6 \pm 0.016
k_d (h $^{-1}$)	0.85 \pm 0.020	1.07 \pm 0.004
model variant I (reversible activation)		
k_a (10^{-7} mL cell $^{-1}$ h $^{-1}$)	10.7 \pm 0.28	4.5 \pm 0.017
k_e (10^{-7} mL cell $^{-1}$ h $^{-1}$)	21.3 \pm 0.99	4.7 \pm 0.043
k_d (h $^{-1}$)	1.01 \pm 0.021	1.08 \pm 0.004
model variant II (irreversible activation) ($N = 7$)		
k_a (10^{-7} mL cell $^{-1}$ h $^{-1}$)	9.2 \pm 0.26	4.4 \pm 0.016
k_e (10^{-7} mL cell $^{-1}$ h $^{-1}$)	22.1 \pm 1.05	5.5 \pm 0.071
k_d (h $^{-1}$)	0.99 \pm 0.019	1.16 \pm 0.008
model variant II (irreversible activation) ($N = 12$)		
k_a (10^{-7} mL cell $^{-1}$ h $^{-1}$)	9.4 \pm 0.26	4.4 \pm 0.016
k_e (10^{-7} mL cell $^{-1}$ h $^{-1}$)	23.2 \pm 1.10	5.4 \pm 0.071
k_d (h $^{-1}$)	1.00 \pm 0.019	1.16 \pm 0.008
model variant III (unsaturated digestion)		
k_a (10^{-7} mL cell $^{-1}$ h $^{-1}$)	6.1 \pm 0.19	4.2 \pm 0.014
k_e (10^{-7} mL cell $^{-1}$ h $^{-1}$)	32.7 \pm 1.72	9.8 \pm 0.098
k_d (h $^{-1}$)	0.49 \pm 0.013	1.22 \pm 0.005

Table 4: Estimates, for the various models, of the kinetic parameters describing engulfment, activation and digestion of apoptotic cells by macrophages. Each parameter estimate is the average of the parameter fits to 5 independent time series (i.e. replicates), with 9 measurements each. The values are given as mean \pm SD, where SD is the standard deviation observed between the parameter fits to the individual replicates.

parameter	Balb/c	NOD
basic model		
k_e (10^{-7} mL cell $^{-1}$ h $^{-1}$)	12.5 \pm 3.20	4.6 \pm 0.69
k_d (h $^{-1}$)	0.81 \pm 0.079	1.13 \pm 0.141
model variant I (reversible activation)		
k_a (10^{-7} mL cell $^{-1}$ h $^{-1}$)	10.8 \pm 3.02	4.6 \pm 0.71
k_e (10^{-7} mL cell $^{-1}$ h $^{-1}$)	18.6 \pm 4.00	4.3 \pm 0.70
k_d (h $^{-1}$)	0.92 \pm 0.088	1.08 \pm 0.125
model variant II (irreversible activation) ($N = 7$)		
k_a (10^{-7} mL cell $^{-1}$ h $^{-1}$)	9.3 \pm 2.68	4.6 \pm 0.66
k_e (10^{-7} mL cell $^{-1}$ h $^{-1}$)	19.5 \pm 3.86	5.3 \pm 0.94
k_d (h $^{-1}$)	0.96 \pm 0.119	1.25 \pm 0.233
model variant II (irreversible activation) ($N = 12$)		
k_a (10^{-7} mL cell $^{-1}$ h $^{-1}$)	9.3 \pm 2.65	4.5 \pm 0.64
k_e (10^{-7} mL cell $^{-1}$ h $^{-1}$)	19.8 \pm 3.88	5.2 \pm 0.94
k_d (h $^{-1}$)	0.95 \pm 0.121	1.24 \pm 0.236
model variant III (unsaturated digestion)		
k_a (10^{-7} mL cell $^{-1}$ h $^{-1}$)	6.4 \pm 2.67	4.1 \pm 0.59
k_e (10^{-7} mL cell $^{-1}$ h $^{-1}$)	25.8 \pm 5.11	9.6 \pm 1.34
k_d (h $^{-1}$)	0.48 \pm 0.107	1.32 \pm 0.254

Table 5: Model comparisons based on the corrected Akaike’s Information Criterion AIC_c (Eqns. (16) and (18)). n = number of observations; K = number of fitted parameters. Models that are most probable have lowest values of AIC_c . (Relative AIC_c values are not significant but the relative Akaike weights, w_i , directly indicate the relative probabilities of the models.) The models that are most likely to be the best description of phagocytosis are the basic model for NOD mice (i.e. macrophages do not get activated), and variant I for Balb/c mice (i.e. macrophages undergo a reversible activation step). It is very unlikely that replicates truly vary in their kinetic parameters, since replicate fits lead to lower relative values of the weights w_i .

Fitting	Model	Strain	SSE	K	n	AIC_c	w_i
replicate	basic model	Balb/c	$2.99 \cdot 10^9$	10	45	837.05	13.73 %
replicate	variant I	Balb/c	$2.22 \cdot 10^9$	15	45	843.68	0.50 %
replicate	variant II ($N = 7$)	Balb/c	$2.24 \cdot 10^9$	15	45	844.08	0.41 %
replicate	variant II ($N = 12$)	Balb/c	$2.34 \cdot 10^9$	15	45	846.04	0.15 %
replicate	variant III	Balb/c	$3.50 \cdot 10^9$	15	45	864.16	0.00 %
concurrent	basic model	Balb/c	$5.56 \cdot 10^9$	2	45	842.74	0.80 %
concurrent	variant I	Balb/c	$4.45 \cdot 10^9$	3	45	835.00	38.14 %
concurrent	variant II ($N = 7$)	Balb/c	$4.53 \cdot 10^9$	3	45	835.86	24.81 %
concurrent	variant II ($N = 12$)	Balb/c	$4.57 \cdot 10^9$	3	45	836.16	21.38 %
concurrent	variant III	Balb/c	$5.82 \cdot 10^9$	3	45	847.07	0.09 %
replicate	basic model	NOD	$1.87 \cdot 10^7$	10	45	608.67	0.06 %
replicate	variant I	NOD	$1.67 \cdot 10^7$	15	45	623.78	0.00 %
replicate	variant II ($N = 7$)	NOD	$1.75 \cdot 10^7$	15	45	625.69	0.00 %
replicate	variant II ($N = 12$)	NOD	$1.75 \cdot 10^7$	15	45	625.75	0.00 %
replicate	variant III	NOD	$1.83 \cdot 10^7$	15	45	627.68	0.00 %
concurrent	basic model	NOD	$2.29 \cdot 10^7$	2	45	595.54	46.13 %
concurrent	variant I	NOD	$2.28 \cdot 10^7$	3	45	597.76	15.16 %
concurrent	variant II ($N = 7$)	NOD	$2.27 \cdot 10^7$	3	45	597.44	17.82 %
concurrent	variant II ($N = 12$)	NOD	$2.27 \cdot 10^7$	3	45	597.39	18.22 %
concurrent	variant III	NOD	$2.47 \cdot 10^7$	3	45	601.28	2.61 %

Figure Captions

Figure 1: An image of the experimental results showing Balb/c macrophages with internalized apoptotic cells. Images such as this were used to quantify the dynamics of macrophage classes for the two mouse strains.

Figure 2: Phagocytosis of apoptotic cells by macrophages from Balb/c vs. NOD mice. Model predictions are compared with experimental data. The graph shows macrophage classes M_0, \dots, M_3 (i.e. total macrophages with 0, \dots , 3 visible engulfed apoptotic cells) on a log plot. Error bars on data points denote standard deviations. We used a maximal macrophage capacity of $N = 7$ apoptotic cells for all models. Parameters were fitted to the data using the Gepasi software and its Marquardt Levenberg method applied to the full set of differential equations. Values of the parameters obtained as best fits are given in Table 3. For variants II and III, classes M_0 and M_u were lumped together to compare with the observed M_0 .

Figure 3: The fitted time dynamics of percent phagocytosis, Φ , and phagocytic index, I_Φ , for the different model variants (each one with macrophage capacity, $N = 7$), for the parameters as given in Table 3. The comparison between Balb/c and NOD is shown. Error bars on data points denote standard deviations.

Figure 4: The time course of all populations predicted by the basic model and variant I (reversible activation). Red curve: $A(t)$ (level of apoptotic cells). Green curve: level of class M_0 macrophages (with no visible engulfed apoptotic cells). Blue curves: levels of macrophage classes M_1, M_2 and M_3 (with 1, 2, or 3 engulfed apoptotic cells).

Figure 5: As in Figure 4 but for model variants II and III (reversible activation and unsaturated digestion, respectively). Red curve: $A(t)$. Green curve: level of class M_u macrophages (resting macrophages with no visible engulfed apoptotic cells). Blue curves: M_1, M_2 and M_3 . Yellow curve: level of class M_0 (activated macrophages without engulfed apoptotic cells).

Figure 6: The dynamics of λ and λ_a in the basic model and variant I (reversible activation), for Balb/c and NOD mice, compared with the QSS estimation of those parameters. Also shown (data points with error bars) are the corresponding values of λ and λ_a based on successive ratios M_{i+1}/M_i directly from experimental data. The thick curves show model predictions of λ based on Eqns. (25) and (40b). In (a) the thin blue lines show the approximation of λ based on the percent phagocytosis, Φ , Eqn. (33); the thin red lines show the approximation based on the phagocytic index, I_Φ , Eqn. (35). In (b), the thin red and green lines show the approximations of λ and λ_a , based on both Φ and I_Φ (Eqns. (48)). In all cases, the approximations become reasonable after a period of approximately 1–3 hours and closely correspond to λ values based on the experimental data.

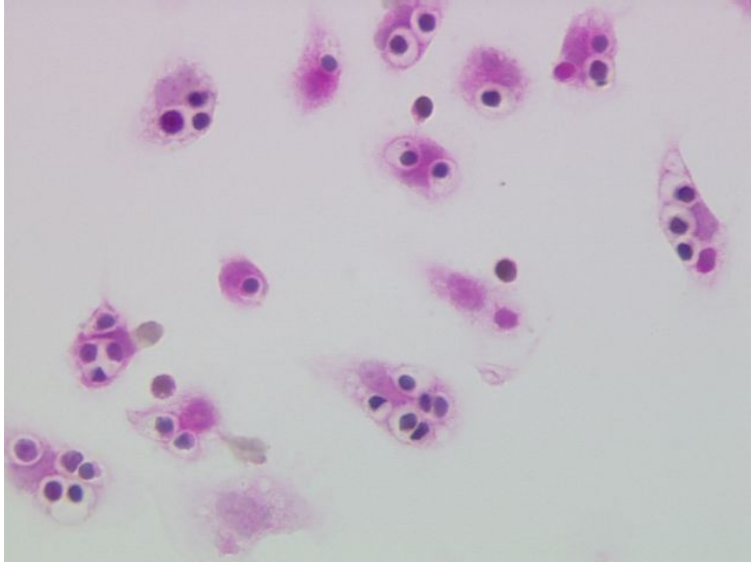
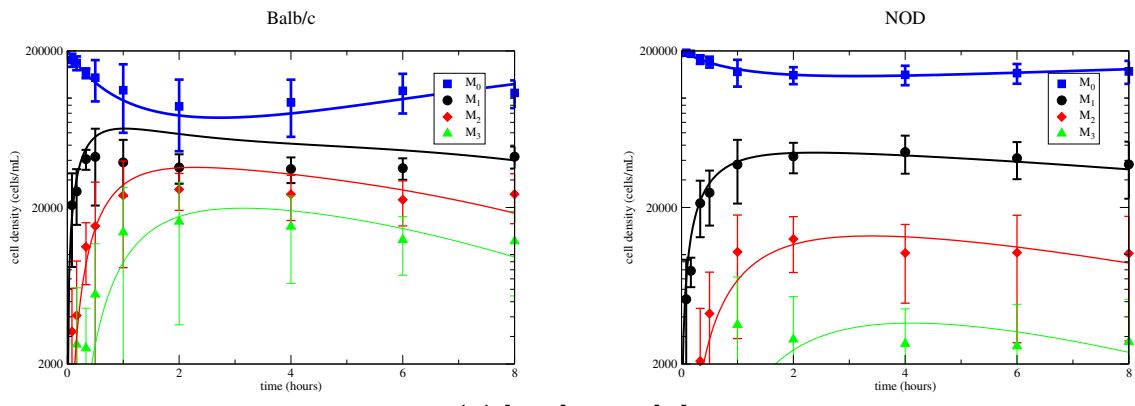
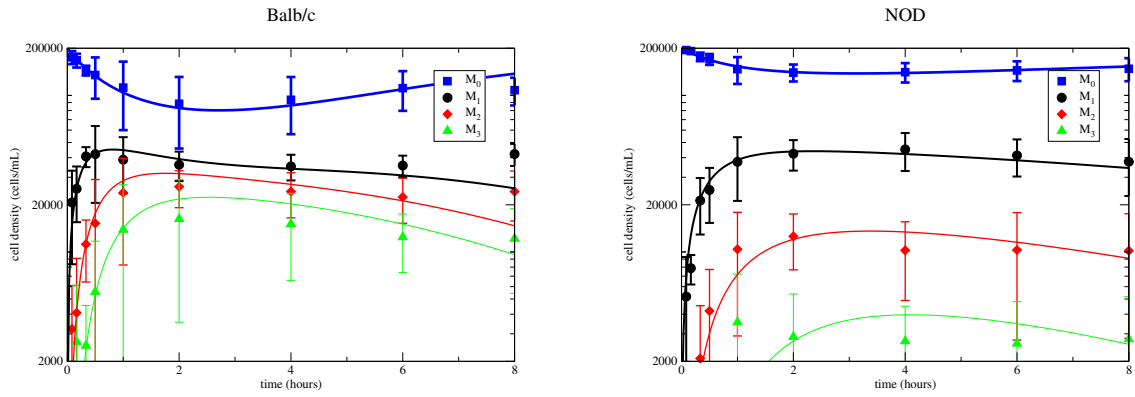


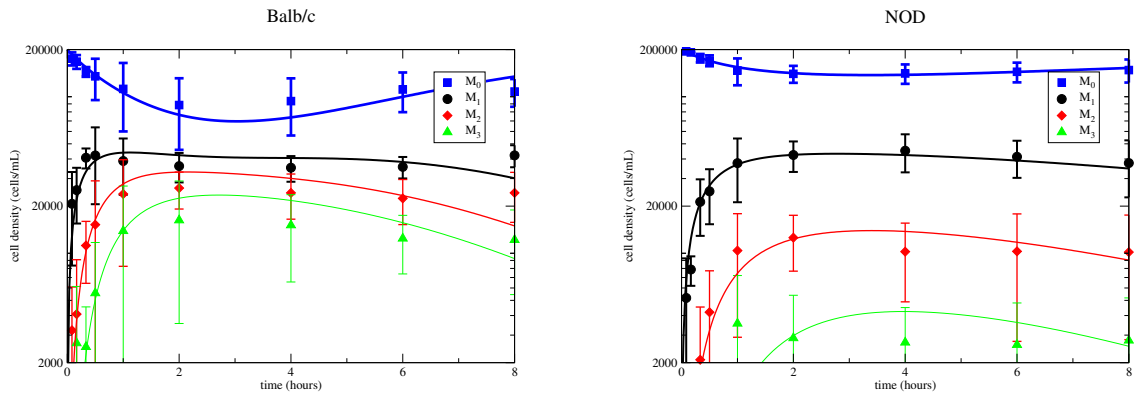
Figure 1



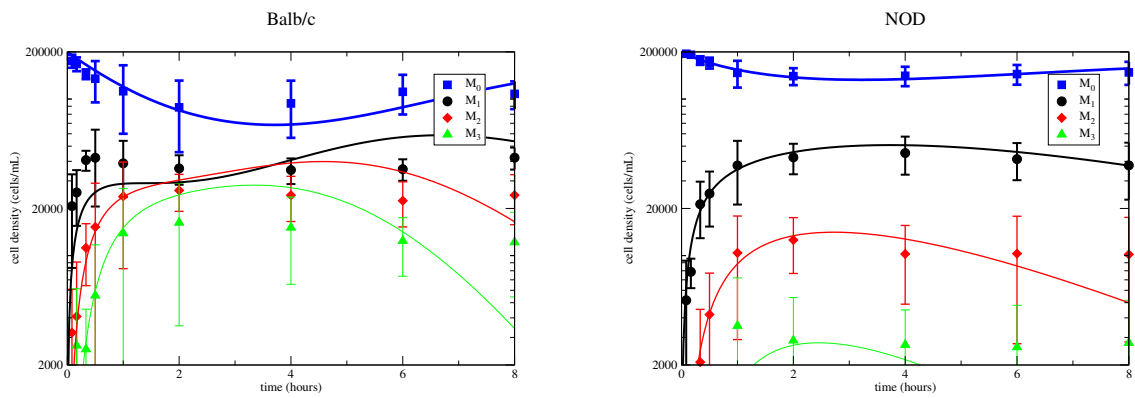
(a) basic model



(b) model variant I (reversible activation)

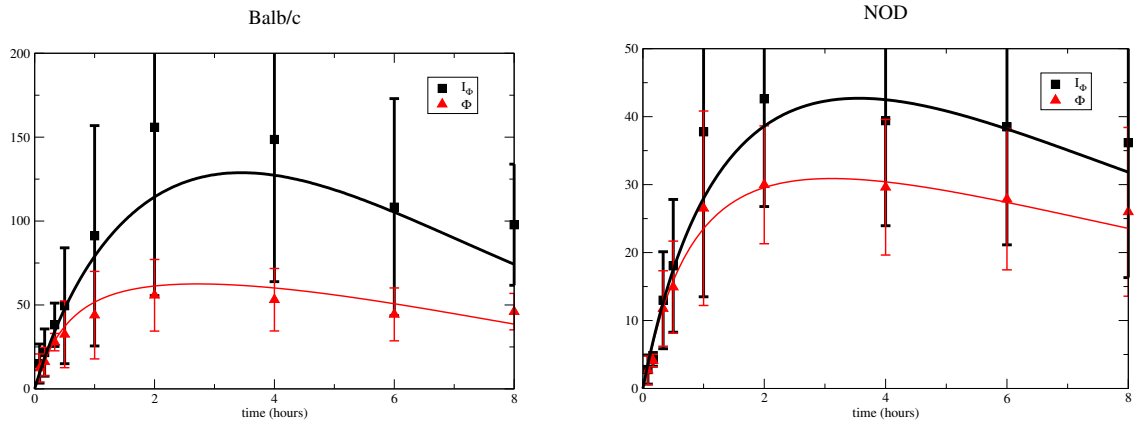


(c) model variant II (irreversible activation)

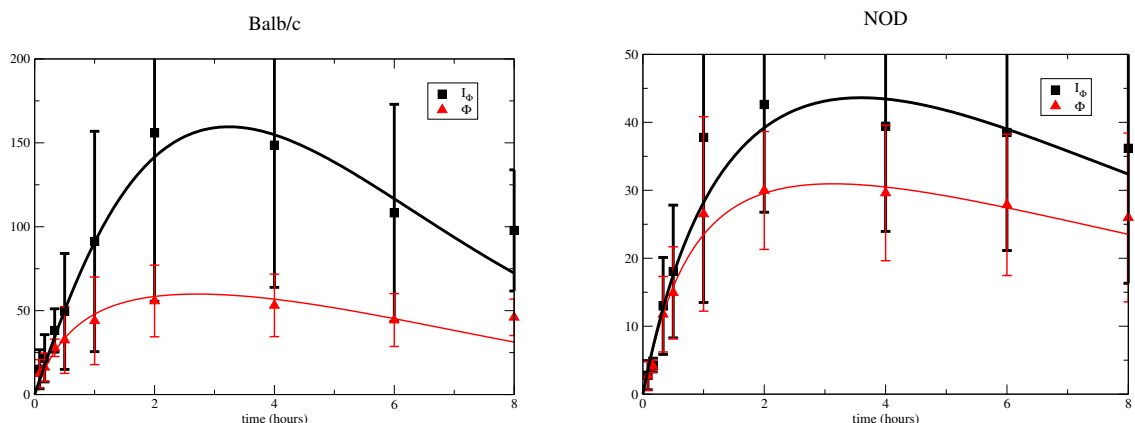


(d) model variant III (unsaturated digestion)

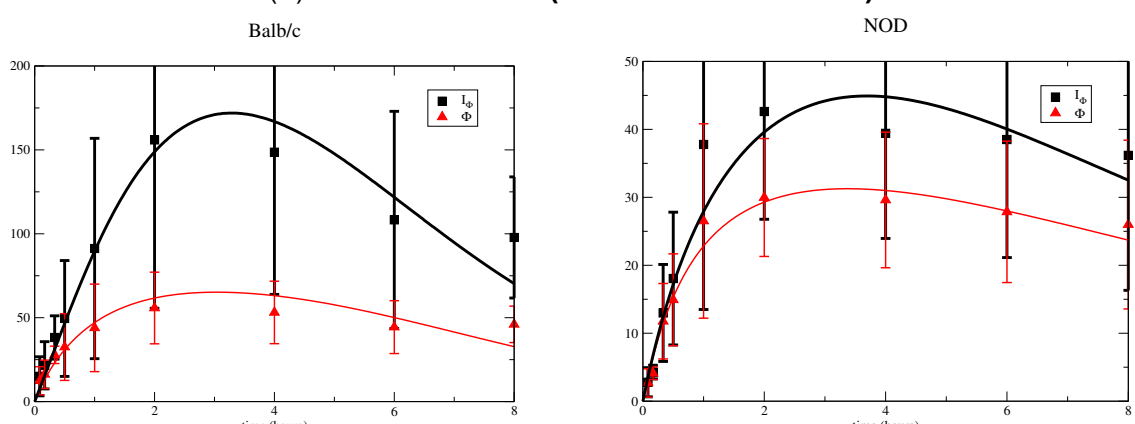
Figure 2



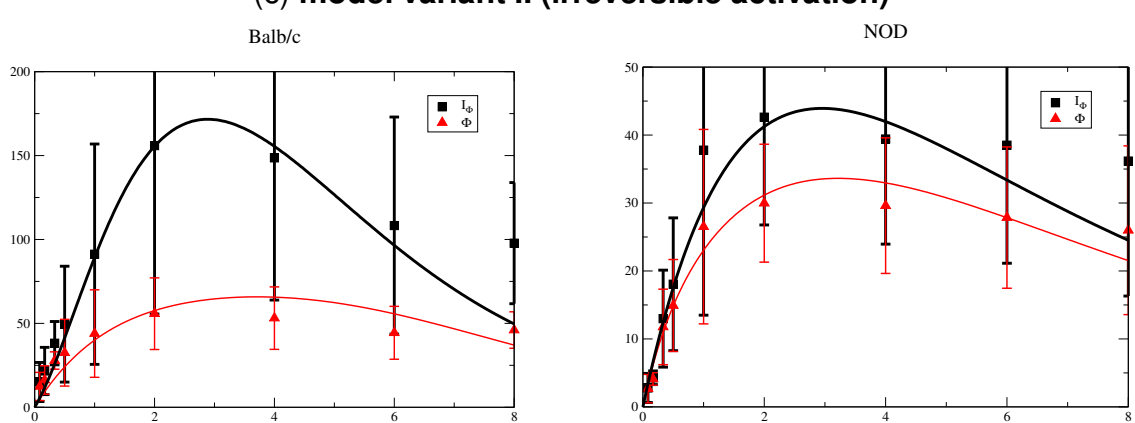
(a) basic model



(b) model variant I (reversible activation)

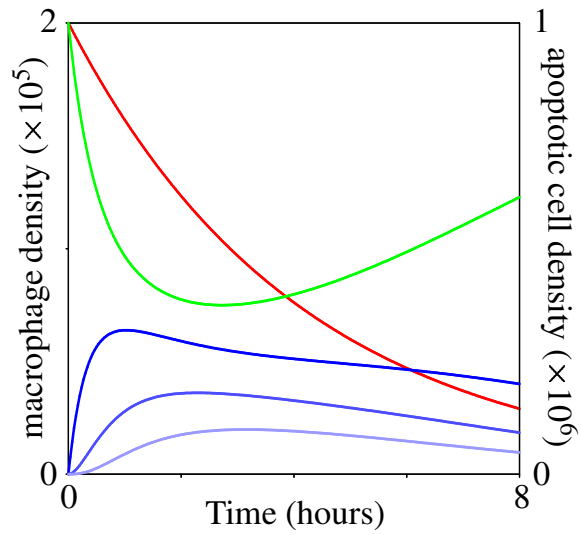


(c) model variant II (irreversible activation)

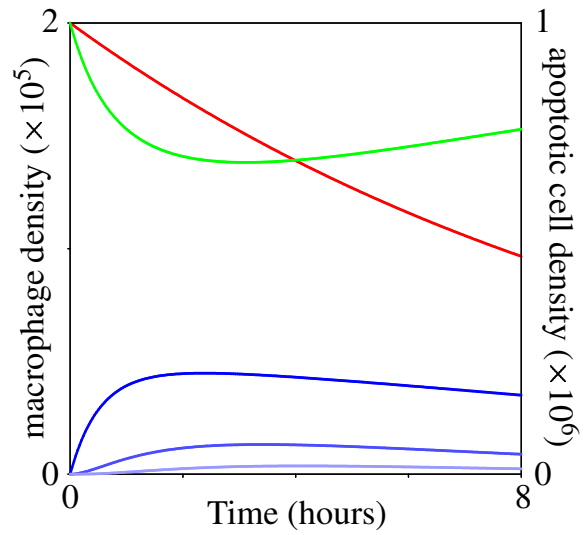


(d) model variant III (unsaturated digestion)

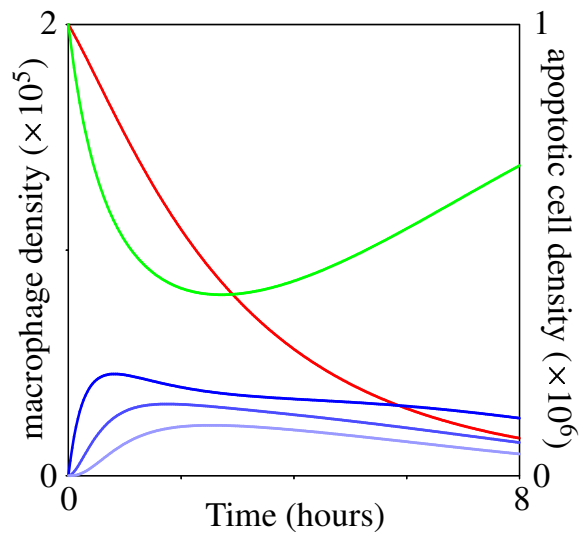
Figure 3



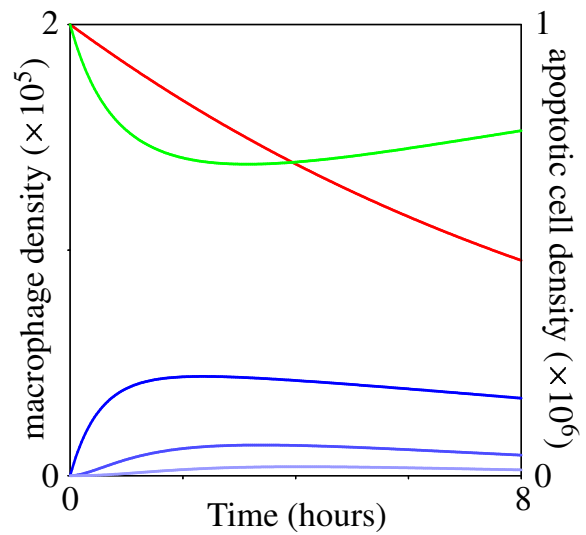
(a) **basic model, Balb/c**



(b) **basic model, NOD**

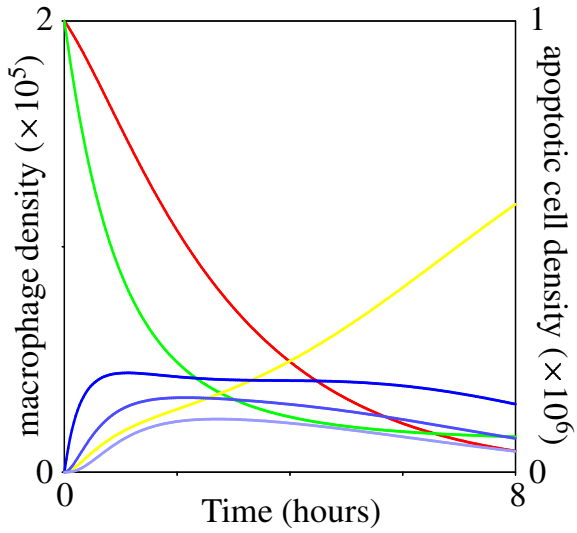


(c) **model variant I, Balb/c**

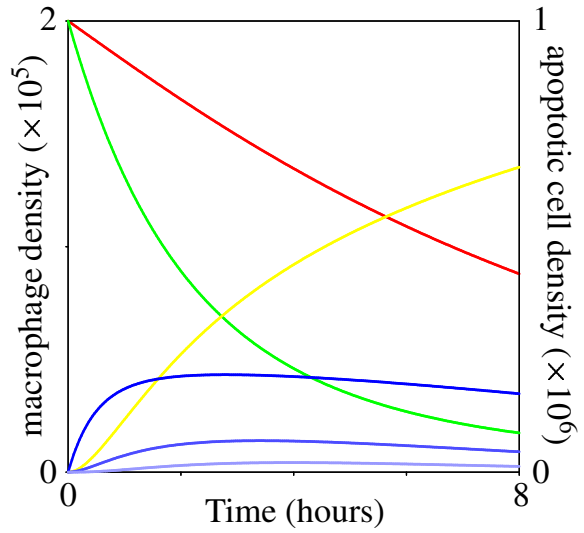


(d) **model variant I, NOD**

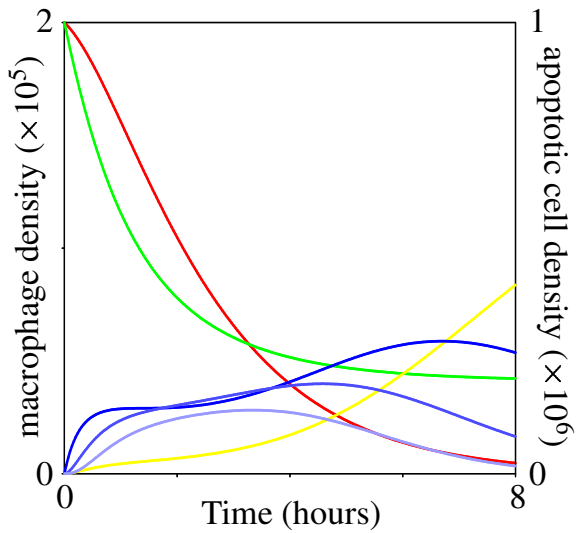
Figure 4



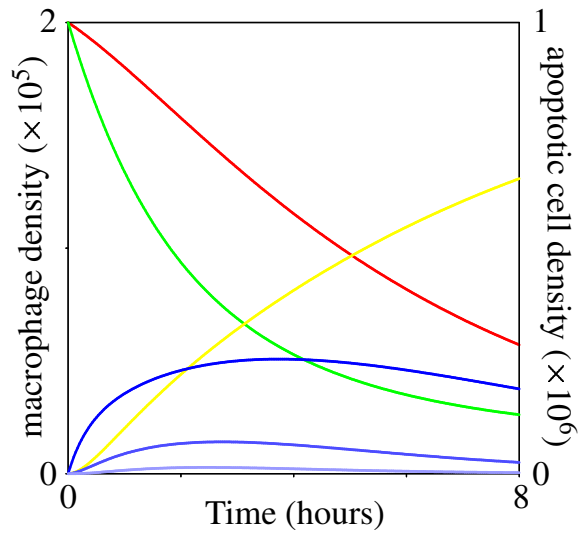
(a) **model variant II, Balb/c**



(b) **model variant II, NOD**

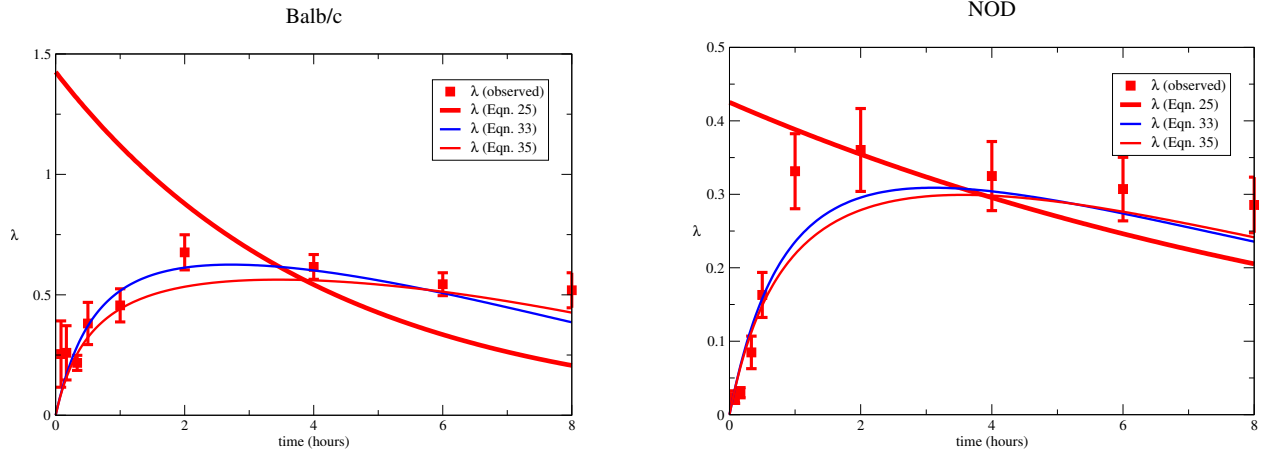


(c) **model variant III, Balb/c**

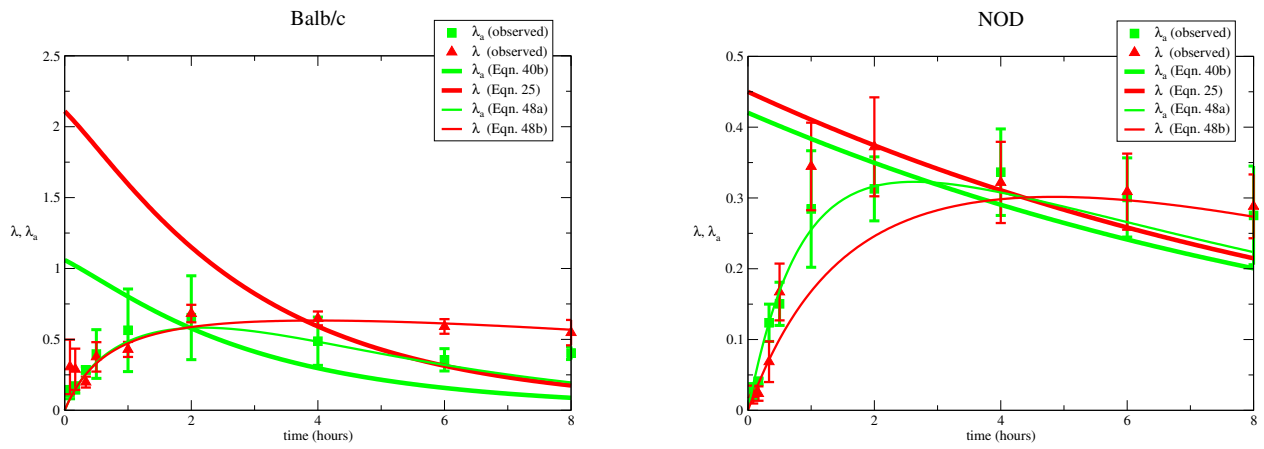


(d) **model variant III, NOD**

Figure 5



(a) basic model



(b) model variant I (reversible activation)

Figure 6